Raman scattering signatures of strong spin-phonon coupling in the bulk magnetic van der Waals material CrSBr

Amit Pawbake,[1,*] Thomas Pelini,[1] Nathan P. Wilson,[2] Kseniia Mosina,[3] Zdenek Sofer,[3] Rolf Heid,[4] and Clement Faugeras[1,†]

[1]*LNCMI, UPR 3228, CNRS, EMFL, Université Grenoble Alpes, 38000 Grenoble, France*
[2]*Walter Schottky Institut, Physics Department and MCQST, Technische Universitat Munchen, 85748 Garching, Germany*
[3]*Chemistry Department, University of Chemistry and Technology Prague, 16628 Prague, Czech Republic*
[4]*Institute for Quantum Materials and Technologies, Karlsruhe Institute of Technology, 76131 Karlsruhe, Germany*

(Received 22 November 2022; revised 29 January 2023; accepted 1 February 2023; published 16 February 2023)

Magnetic excitations in layered magnetic materials that can be thinned down to the two-dimensional (2D) monolayer limit are of great interest from a fundamental point of view and for applications. Raman scattering has played a crucial role in exploring the properties of magnetic layered materials and, even though it is essentially a probe of lattice vibrations, it can reflect magnetic ordering in solids through the spin-phonon interaction or through the observation of magnon excitations. In bulk CrSBr, a layered *A*-type antiferromagnet (AF), we show that the magnetic ordering can be directly observed in the temperature dependence of the Raman scattering response (i) through the variations of the scattered intensities, (ii) through the activation of new phonon lines reflecting the change of symmetry with the appearance of the additional magnetic periodicity, and (iii) through the observation below the Néel temperature (T_N) of second-order Raman scattering processes. We additionally show that the three different magnetic phases encountered in CrSBr, including the recently identified low-temperature phase, have a particular Raman scattering signature. This work demonstrates that magnetic ordering can be observed directly in the Raman scattering response of bulk CrSBr with in-plane magnetization and that it can provide unique insight into the magnetic phases encountered in magnetic layered materials.

DOI: 10.1103/PhysRevB.107.075421

I. INTRODUCTION

Layered materials that can be thinned down to the monolayer limit and present magnetic properties have emerged as platforms to engineer and investigate exotic magnetic ground states in low dimensions [1]. The observation of long-range magnetic order in two dimensional monolayers of CrI_3 [2] and of $Cr_2Ge_2Te_6$ [3] have triggered a large number of investigations aiming at finding other layered magnetic two-dimensional (2D) materials and at using them within van der Waals (vdW) heterostructures. Magnetic layered materials can be used to introduce magnetic properties through proximity effects [4,5], and for spintronics applications such as spin valves and filters. They are also foreseen as potential building blocks for composite qubits for quantum technologies [6]. These layered magnetic materials present a broad variety of magnetic orders with intra- and interlayer ferro- or antiferromagnetic interactions. Taking into account the variety of possible antiferromagnetic states (Néel-like, zigzag, stripe), there is a need to establish experimental techniques sensitive to these different orders and symmetries. Within this broad family of materials, CrSBr has recently stimulated great interest because this material can be thinned down to the monolayer with persisting magnetic properties and, in contrast to CrX_3 or VX_3 compounds (where X = I, Br, or Cl), bulk CrSBr is stable in air and can hence be manipulated in standard conditions [7].

The crystal structure of bulk CrSBr is orthorhombic (see Fig. 1) with space group *Pmmn* (D_{2h}) and no structural phase transitions between 15 and 300 K [7]. From optoelectronics perspectives, it is a direct band-gap semiconductor with $E_g = 1.5$ eV and hosts tightly bound excitons that give rise to photoluminescence signals close to 1.3 eV [7,8]. The electronic properties of CrSBr are strongly anisotropic and this is reflected in its optical [8,9] and transport properties [10]. From these different viewpoints, this material can be seen as a quasi-1D system. CrSBr is a layered material with strong ferromagnetic intralayer interactions which align the Cr^{3+} spins within the plane of the layers, along the crystallographic *b* axis (easy axis); see Fig. 1. This intralayer ferromagnetic order appears below $T_C = 160$ K for bulk samples [11]. The Cr^{3+} ions couple antiferromagnetically across the van der Waals gap and bulk CrSBr is an *A*-type antiferromagnet with $T_N = 133$ K [12], as evidenced by magnetization and magnetotransport [7] investigations. In between T_C and T_N, bulk CrSBr is in an intermediate magnetic phase (iFM) in which the intralayer ferromagnetic order is well established while the interlayer ordering is only partial, comprising both ferro- and antiferromagnetic interlayer couplings [11,13]. When lowering the temperature below $T^* = 40$ K, a change of sign of the magnetoresistance with a simultaneous increase of the magnetization [14] and muon spin relaxation experiments [15]

*amit.pawbake@lncmi.cnrs.fr
†clement.faugeras@lncmi.cnrs.fr

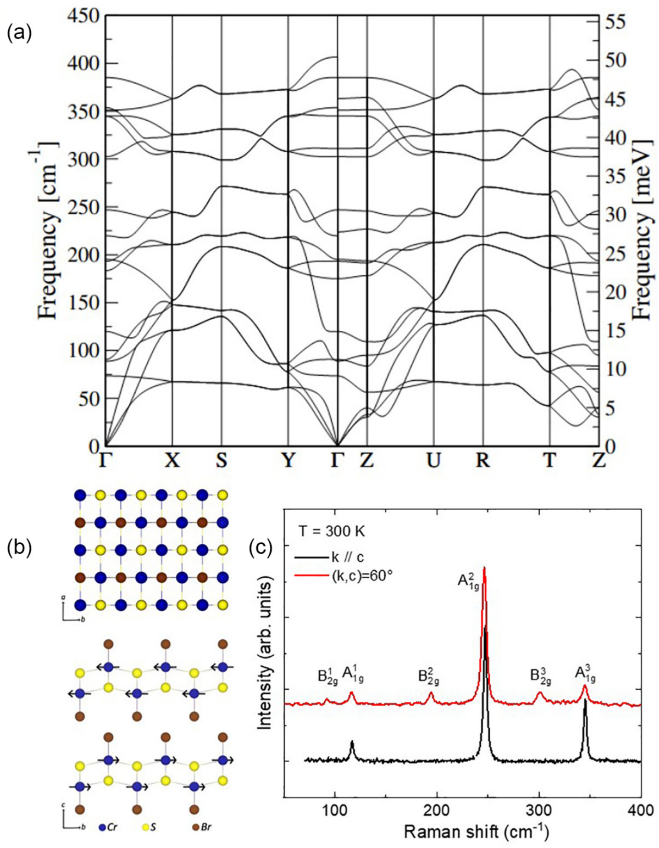

FIG. 1. (a) Calculated phonon band structure of bulk CrSBr at $T = 10$ K. (b) Crystal structure of CrSBr as seen along the c or a crystallographic axis. The arrows represent the magnetic moments aligned in the plane of the layers. Schematic created using VESTA software [29]. (c) Room temperature Raman spectra of bulk CrSBr in perpendicular configuration (black curve) or with a tilt angle of 60° between the light propagation direction and the normal to the surface of the crystal (red curve).

have pointed toward a new magnetic phase. The details of this phase are still under debate and it has been attributed either to the ferromagnetic ordering of magnetic defects within the bulk crystal [14,16] or, alternatively, to a gradual decrease of spin fluctuations below $T = 100$ K leading to a spin freezing process at $T^* = 40$ K with potentially the formation of domains with different magnetic ground states [15].

Antiferromagnetic magnon excitations [17] in bulk CrSBr and their dispersion when applying external magnetic fields have been measured recently with electron paramagnetic resonance (EPR) spectroscopy [18] or through their coupling to excitons in time-resolved reflectivity spectroscopy [19]. The magnon spectrum at $B = 0$ T is composed of two excitations at 25 and 35 GHz reflecting the biaxial magnetic anistotropy of CrSBr. If the direct magnon absorption measured in EPR is well understood, the coupling of magnons to excitons through the strain field induced by the heating due to a pump pulse implies the magnetoelastic interaction and phonons of bulk CrSBr. These measurements provide qualitatively similar behaviors but different energies for magnons [19] than those extracted from direct absorption [18], leading to significantly different microscopic magnetic parameters. A detailed understanding of this interaction hence appears essential to describe the magnetic properties of materials with in-plane magnetization, for which standard Kerr effect measurements, mostly sensitive to the M_z component of the magnetization, can hardly be applied and alternative approaches have to be implemented.

In this article, we use Raman scattering spectroscopy to detect the magnetic phase transitions in bulk CrSBr when lowering temperature. By tilting the sample with respect to the excitation light propagation direction, we activate Raman scattering from phonons at the Z point of the Brillouin zone which are particulary sensitive to the AF ordering along the c axis. The strong spin-lattice coupling is evidenced through the appearance of new phonon modes when the additional magnetic periodicity develops below T_N and by pronounced variations of the scattered intensity. These changes in the Raman scattering spectrum allow identification of the intermediate magnetic phase when $T_C > T > T_N$, the AF order, and also the hidden order phase below T^*. We show that the evolution of phonon modes when lowering temperature from room temperature down to liquid helium temperature cannot be described by usual lattice dynamics [20] and strongly reflects the magnetic ordering and the different magnetic phases in this bulk compound. Additionally, we apply an external magnetic field which effectively modifies the Raman scattering response, further demonstrating the spin-phonon coupling in bulk CrSBr.

II. METHODS

A. Samples and experimental setup

The CrSBr single crystals were synthesized through a chemical vapor transport (CVT) method. Chromium, sulfur, and bromine in a stoichiometric ratio of CrSBr were added and sealed in a quartz tube under a high vacuum (50 g of CrBrS with 0.1% Br excess, ampoule size 50 × 250 mm). The tube was then placed into a two-zone tube furnace. The prereaction was done in crucible furnace where one end of ampoule was kept below 300 °C and bottom was gradually heated to 700 °C over a period of 50 h. Then, the source and growth ends were kept at 800 and 900 °C, respectively. After 25 h, the temperature gradient was reversed, and the hot end gradually increased from 850 to 920 °C over 10 days. High-quality CrSBr single crystals with lengths up to 2 cm were achieved. Bulk CrSBr was placed on the cold finger of a variable temperature helium flow cryostat. We use a long working distance optical objective with numerical aperture of 0.55 to excite the sample and collect Raman scattering signals. Raman scattering signals were analyzed by a grating spectrometer equipped with a nitrogen-cooled silicon charge coupled device (CCD). We use a depolarizer to excite with unpolarized excitation and to detect the unpolarized Raman scattering response. Measurements were performed at liquid helium temperature with a $\lambda = 633$ nm excitation from solid-state laser diodes, keeping the optical power below 0.3 mW. For magneto-Raman or magnetophotoluminescence measurements, we have used a homemade experimental setup based on free beam propagation of optical excitation and collection. We use a long working distance objective with a numerical

aperture $NA = 0.35$ used to focus the excitation beam down to a spot size of 1 μm and to collect Raman scattering or photoluminescence signals. The sample was placed on piezo motors, allowing for the spatial mapping of the optical response. This setup is then inserted into a closed metallic tube filled with helium exchange gas and then placed at liquid helium temperature in a superconducting solenoid producing magnetic fields up to $B = 14$ T.

B. Theory

Lattice dynamics properties for orthorhombic CrSBr were calculated using the linear response or density-functional perturbation theory (DFPT) implemented in the mixed-basis pseudopotential method [21,22]. The electron-ion interaction is described by norm-conserving pseudopotentials, which were constructed following the descriptions of Vanderbilt [23]. Semicore states Cr-3*s* and Cr-3*p* were included in the valence space. In the mixed-basis approach, valence states are expanded in a combination of plane waves and local functions at atomic sites, which allows an efficient description of more localized components of the valence states. Here, plane waves with a cutoff for the kinetic energy of 24 Ry and local functions of *s*, *p* types for S and Br and *s*, *p*, *d* types for Cr, respectively, were employed. Spin-polarized calculations were done for both the small cell, assuming a ferromagnetic (FM) ground state, and a $1 \times 1 \times 2$ supercell with an antiferromagnetic (AFM) ground state. Brillouin-zone integration was performed by sampling a $12 \times 8 \times 4$ *k*-point mesh for the FM cell and a $12 \times 8 \times 2$ (AFM) *k*-point mesh for the AFM cell, respectively. The exchange-correlation functional was represented by the general-gradient approximation (GGA) in the PBE form [24].

Within GGA, the ground state of CrSBr in the magnetic state is insulating, albeit with a rather small gap size of 0.3 eV, as compared to the experimental optical gap of 1.25 eV [7]. To improve on the gap size, correlations at the Cr site were incorporated in the DFT+U scheme. Following previous publications [25–27], we used $U = 4$ eV and $J = 1$ eV (corresponding to $U_{\text{eff}} = U - J$ of 3 eV), thereby increasing the gap to 1.3 eV. The main effect of the $+U$ correction on the phonons was a hardening in particular of the high-frequency modes due to a reduced electronic screening.

Lattice constants for the orthorhombic structure were taken from measurements at $T = 10$ K by Lopez-Paz *et al.* ($a = 3.51069$ Å, $b = 4.74623$ Å, $c = 7.9162$ Å) [15]. Internal structural parameters were relaxed until the atomic forces were smaller than 2.6×10^{-2} eV/Å. Above-mentioned calculational parameters guaranteed convergence of phonon frequencies better than 1 cm^{-1}. Comparison of phonons for the FM and AFM cell showed that the difference in magnetic structure has hardly any effect on phonon frequencies. The main difference is a folding of the *Z*-point phonons of the FM cell to the Γ point of the AFM phase. This renders some of the cell modes at *Z* (FM) to become Raman active in the AFM phase. Full phonon dispersion for the FM cell was calculated by performing DFPT calculations of dynamical matrices on a $4 \times 4 \times 2$ momentum mesh and subsequently using standard Fourier interpolation to obtain dynamical matrices throughout the Brillouin zone. To correctly describe the Longitudinal Optical / Transverse Optical (LO/TO) splitting of infrared active modes, the nonanalytic part of the dynamical matrices was included following the procedure outlined in Ref. [28]. It does not affect the Raman modes.

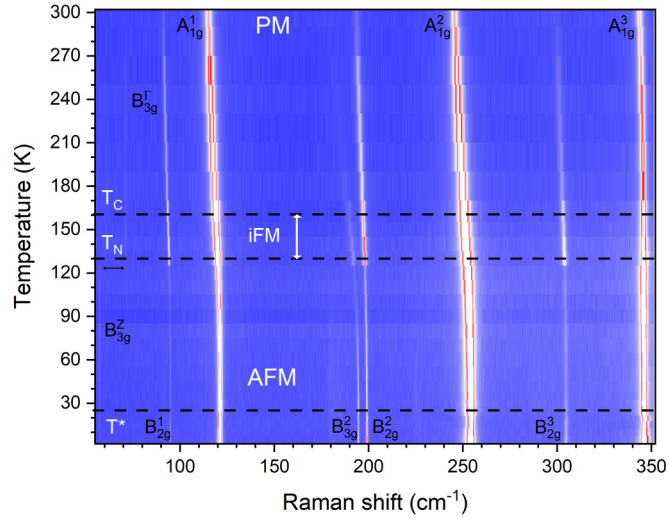

FIG. 2. False color map of the unpolarized Raman scattering response of bulk CrSBr as a function of temperature. The different magnetic phases are indicated, the paramagnetic phase (PM), the intermediate magnetic phase (iFM), and the antiferromagnetic phase (AF), together with the critical temperatures T_N and T^* and the different phonon symmetries.

III. RESULTS AND DISCUSSION

The primitive cell of bulk CrSBr includes 6 atoms in the high-temperature paramagnetic phase and 12 atoms in the AF super cell ($1 \times 1 \times 2$) below T_N. The phonon spectrum includes 15 optical modes and 3 acoustical branches. The calculated phonon Brillouin zone for bulk CrSBr is presented in Fig. 1(a). When measured in back scattering geometry with the incident light perpendicular to the surface, the unpolarized first-order Raman scattering spectrum of bulk CrSBr is composed of three main contributions at 117, 257, and 345 cm^{-1}, respectively [see Fig. 1(c)]. They arise from Γ-point optical phonons of A_{1g} symmetry, with atomic displacements pattern perpendicular to the plane of the layers. When imposing a 60° tilt angle to the sample, three new contributions appear in the room-temperature Raman scattering response at 92, 194, and 301 cm^{-1}, which correspond to the three B_{2g} modes at the Γ point, with atomic displacements in the plane of the layers. The atomic displacements associated with all the phonon modes of bulk CrSBr are presented in Fig. S1 of the Supplemental Material [30].

The experimentally observed evolution of phonon energies in CrSBr as a function of temperature, presented in Fig. 2, clearly goes beyond phonon evolutions observed in semiconducting 2D materials [20]. When lowering temperature, anharmonicity effects lead to a decrease of the phonons linewidths and to an increase of the phonons energies [31,32] with a dependence that reflects multiphonon processes and that, in a first approximation, takes the form $\omega(T) = \omega_0 + c_i\langle n_i\rangle$, where $\langle n_i\rangle$ is the temperature-dependent population

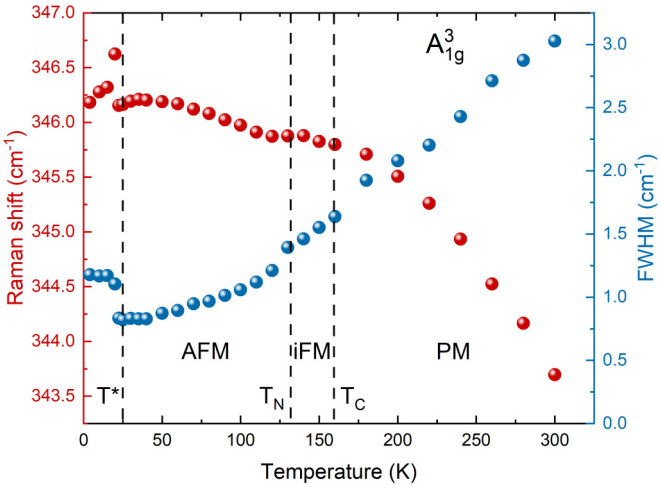

FIG. 3. Evolution of the A^3_{1g} phonon energy (red points) and linewidth (blue points) as a function of temperature. The errors are smaller than the symbol size.

of phonons with energy ω_i and c_i is a numerical factor [32]. At $T = 5$ K, the three main Raman scattering features corresponding to the $A^{1,2,3}_{1g}$ phonons are observed at 121, 254, and 346 cm^{-1}, respectively. A comparison between experimental and calculated phonon energies is presented in Table S1 of the Supplemental Material [30]. Let us first investigate the evolution of the A^3_{1g} phonon with temperature presented in Fig. 3. Below T_N, CrSBr becomes magnetically ordered and the spin-spin interaction is modified by propagating phonons that can change the superexchange angles and the resulting the magnetic exchange couplings [33]. This interaction might also slightly modify the lattice constant and phonon energies [27]. We observe a hardening of the phonon mode from room temperature down to T_C where the phonon energy stays rather constant down to T_N. This temperature range corresponds to the intermediate magnetic phase in which the intralayer ferromagnetism is established, but spins in adjacent layers are not all AF ordered [11,13]. For lower temperatures, the A^3_{1g} phonon mode hardens again before showing a sharp discontinuity around $T = 25$ K which coincides with the transition to a new magnetic ground state [14,15]. The evolution of the full width at half maximum (FWHM) of the A^3_{1g} phonon presented in Fig. 3 also deviates from expectations considering only anharmonicity: The FWHM decreases when lowering temperature but shows an inflection point in the intermediate magnetic phase, around $T = 140$ K. We understand this behavior as a combined effect of anharmonicity with the reduction of the phonon thermal populations and of the simultaneous reduction of spin fluctuations of the magnetic ions [15], which leads to the suppression of a phonon scattering mechanism and to a decrease of the linewidth. Close to $T = 25$ K, we observe a sharp increase of the FWHM of the A^3_{1g} phonon. The evolution of both the energy and of the FWHM of the A^3_{1g} phonon hence reflects the details of the magnetic ordering in this bulk magnetic van der Waals material, revealing the four magnetic phases discovered in bulk CrSBr.

In addition to these effects, particularly pronounced for the A^3_{1g} phonon mode [34], the emergence of magnetism in bulk CrSBr and the spin-phonon coupling also has profound implications on the overall Raman scattering response. As can be seen in Fig. 2, the scattered intensity from the different phonon modes increases significantly for $130\,\text{K} < T < 160\,\text{K}$, which corresponds to the intermediate magnetic phase. We present in the Supplemental Material [30] the evolution of the energies, width, and integrated intensities of all observed Raman scattering features; see Figs. S2–S4. The evolution of the phonon energies goes beyond effects of crystal anharmonicity and most of the peaks show intensity anomalies corresponding to the iFM phase when $T_N < T < T_C$. The increase of full width below $T = 25$ K, particularly marked on the A^3_{1g} phonon, is also observable on A^2_{1g} but not on the A^1_{1g} phonon. The increase of the scattered intensity in the iFM phase affects most of the phonon modes (see Supplemental Material Figs. S4 and S5 [30]).

When the interlayer AF order builds up, the symmetry of the solid changes due to the additional magnetic periodicity imposed on the crystallographic one. In bulk CrSBr, the unit cell doubles along the c axis, which causes the folding of Z-point phonons on the Γ point and the activation of new phonon modes in the Raman scattering response. This effect can be clearly seen with the gradual appearance, for temperatures close to T_C, of an additional phonon peak close to 194 cm^{-1} which we identify as the B_{3g} phonon from the Z point. Additionally, a weak Raman scattering mode at 71 cm^{-1} is observed below $T = 260$ K and corresponds to a B_{3g} phonon from the Γ point. At $T = 130$ K, this mode disappears and a new mode rises at 57 cm^{-1}; see Fig. 4(a). We identify this new mode as the B_{3g} mode from the Z point, activated below T_N. To further reenforce our interpretation that the appearance this phonon below T_N is related to the AF order, we have applied a magnetic field at low temperature. The sample in its AF phase and the c axis is tilted by 30° with respect to the light propagation direction and to the external magnetic field. As the bulk sample is not oriented in the (a, b) plane, we have simultaneously measured the photoluminescence from excitons in bulk CrSBr, which have been shown to be a probe of the saturation field [8] above which all the spins are aligned along the direction of the external magnetic field. These results are shown in Figs. 4(b)–4(d) for the unpolarized magnetophotoluminescence and magneto-Raman scattering, respectively. When measuring the magneto-Raman scattering response, we observe that the 57 cm^{-1} mode observed in the AF phase gradually disappears when the saturation field is reached, in our tilted configuration for $B > 0.8$ T, and the 71 cm^{-1} phonon mode is recovered. Simultaneously, the B^2_{2g} phonon observed at 305 cm^{-1} strongly gains in intensity for $B > 0.8$ T. This magnetic field corresponds to the saturation magnetic field extracted from magnetophotoluminescence and presented in Fig. 4(b), confirming that observing the B_{3g} from the Z point at 57 cm^{-1} is a characteristic signature of the AF phase. The results presented in Figs. 4(c) and 4(d) hence clearly relate the evolution of the Raman scattering response to the magnetic ordering in bulk CrSBr. Puzzling is the complete disappearance of the B_{3g} phonon from the Γ point below T_N accompanied by the strong reduction of intensity of the B_{2g}

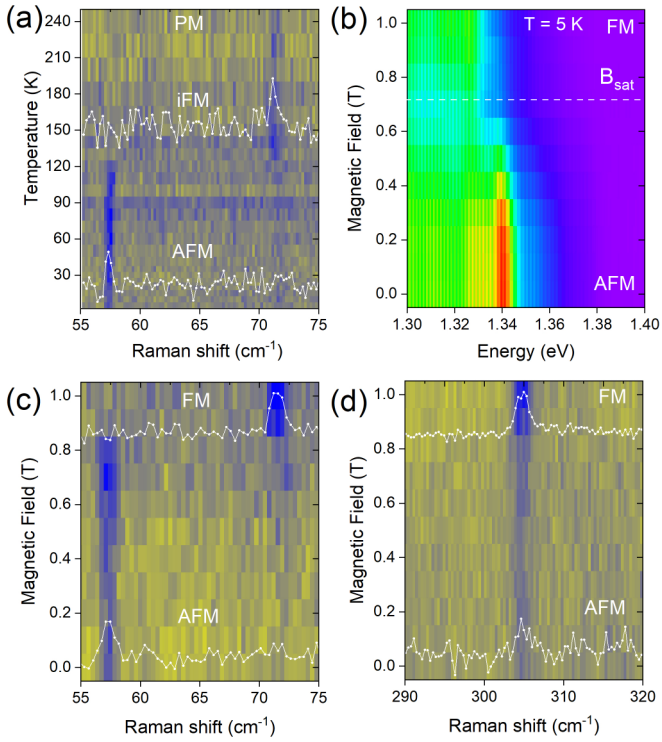

FIG. 4. (a) Evolution of the unpolarized Raman scattering response measured at various temperatures between $T = 5\,\mathrm{K}$ up to $T = 250\,\mathrm{K}$, (b) magnetophotoluminescence of bulk CrSBr up to $B = 1\,\mathrm{T}$ with the B field applied 30° from the c axis and showing a saturation field of $B_{\mathrm{sat}} = 0.75\,\mathrm{T}$, and [(c), (d)] magneto-Raman scattering response at $T = 5\,\mathrm{K}$ with the B field applied in the same configuration as in panel (b) for two different energy windows centered on the B_{3g} phonon mode (c) and on the B_{2g} phonon modes (d).

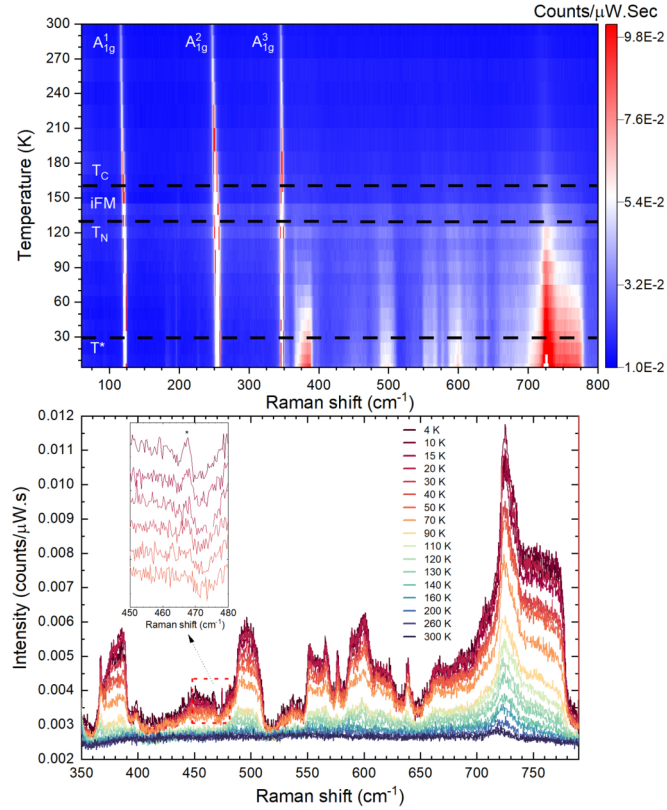

FIG. 5. Top: False color map of the Raman scattering response of bulk CrSBr as a function of temperature showing both the first- and second-order Raman scattering spectrum. Bottom: Raman scattering spectra at different temperatures above and below T_N. The inset focuses on the peak at 467 cm^{-1} (indicated by a star) that appears below T^*.

phonon from the Γ point at 290 cm^{-1}. In the case of phonon zone folding due to the additional magnetic periodicity below T_N, one would expect the appearance of new phonon modes in the Raman scattering response of the magnetic phase, but phonons already active in the high-temperature phase are expected to persist, which is not the case in bulk CrSBr, pointing toward a more complex process.

When the magnetic order appears in bulk CrSBr, the first-order Raman scattering spectrum is profoundly changed as described above, but we also observe the appearance of the second-order Raman scattering spectrum. This evolution is presented in Figs. 5(a) and 5(b). The second order appears when the temperature is tuned below 160 K, which corresponds to the establishment of the intralayer ferromagnetic order and grows in intensity when temperature is further decreased. It extends from 370 to 780 cm^{-1} and includes several broad features, with FWHM in the range of 20–30 cm^{-1} which correspond to multiphonon processes, including acoustical phonons at the Z and X points of the phonon Brillouin zone [see Fig. 1(a)]. The appearance of the second-order spectrum when decreasing temperature is related to a growing resonance of the laser energy, in this case $E_{\mathrm{exc}} = 1.96\,\mathrm{eV}$, with the B exciton energy at 1.82 eV.

We have previously described the sharp increase of the energy and linewidth of the A^3_{1g} phonon below $T = 25\,\mathrm{K}$. The low-temperature magnetic phase has another Raman scattering signature within this second-order spectrum. As we show in the inset of Fig. 5(b), we observe at $E = 467$ cm^{-1} an additional sharp Raman scattering peak with FWHM = 2 cm^{-1} that can only be observed at the lowest temperatures, when $T < 40\,\mathrm{K}$. This peak appears at an energy higher than that of the first-order spectrum and can hence hardly be assigned to the activation of a previously forbidden scattering. It should rather be a multiphonon process involving, for instance, the simultaneous emission of A^1_{1g} and A^3_{1g} phonons. Additionally, this feature does not show any dependence on the applied magnetic field (see the Supplemental Material Fig. S6). We cannot conclude with the present data on the origin of this new mode which appears as characteristic of the low-temperature magnetic phase in bulk CrSBr.

IV. CONCLUSIONS

To conclude, using temperature- and magnetic-field-dependent Raman scattering techniques, we have described the strong spin-phonon coupling in bulk CrSBr. The different magnetic phases have distinct Raman scattering signatures that experiments performed in a tilted geometry allow to precisely trace and investigate. Our *ab initio* calculations of the

phonon band structure in the AF phase agree well with the Raman scattering experiments and allow for the identification of the different phonon modes. We have shown the Raman scattering signatures of the still-debated magnetic phase at low temperature in the form of discontinuities in the temperature evolution of the energy and linewidth of the A_{1g}^3 phonon mode, in the appearance of a new Raman scattering peak at $E = 467\ \mathrm{cm}^{-1}$. Raman scattering techniques are very efficient to get insights into the rich magnetic phases of magnetic layered materials with arbitrary magnetization direction.

ACKNOWLEDGMENTS

We acknowledge technical support from I. Breslavetz. This work has been partially supported by the EC Graphene Flagship project. N.P.W. acknowledges support from the Deutsche Forschungsgemeinschaft (DFG, German Research Foundation) under Germany's Excellence Strategy EXC-2111-390814868. Z.S. was supported by Project No. LTAUSA19034 from Ministry of Education Youth and Sports (MEYS). R.H. acknowledges support by the state of Baden-Württemberg through bwHPC.

[1] Q. H. Wang, A. Bedoya-Pinto, M. Blei, A. H. Dismukes, A. Hamo, S. Jenkins, M. Koperski, Y. Liu, Q.-C. Sun, E. J. Telford, H. H. Kim, M. Augustin, U. Vool, J.-X. Yin, L. H. Li, A. Falin, C. R. Dean, F. Casanova, R. F. L. Evans, M. Chshiev *et al.*, The magnetic genome of two-dimensional van der Waals materials, ACS Nano **16**, 6960 (2022).

[2] B. Huang, G. Clark, E. Navarro-Moratalla, D. R. Klein, R. Cheng, K. L. Seyler, D. Zhong, E. Schmidgall, M. A. McGuire, D. H. Cobden, W. Yao, D. Xiao, P. Jarillo-Herrero, and X. Xu, Layer-dependent ferromagnetism in a van der Waals crystal down to the monolayer limit, Nature (London) **546**, 270 (2017).

[3] C. Gong, L. Li, Z. Li, H. Ji, A. Stern, Y. Xia, T. Cao, W. Bao, C. Wang, Y. Wang, Z. Q. Qiu, R. J. Cava, S. G. Louie, J. Xia, and X. Zhang, Discovery of intrinsic ferromagnetism in two-dimensional van der Waals crystals, Nature (London) **546**, 265 (2017).

[4] D. Zhong, K. L. Seyler, X. Linpeng, R. Cheng, N. Sivadas, B. Huang, E. Schmidgall, T. Taniguchi, K. Watanabe, M. A. McGuire, W. Yao, D. Xiao, K.-M. C. Fu, and X. Xu, Van der Waals engineering of ferromagnetic semiconductor heterostructures for spin and valleytronics, Sci. Adv. **3**, e1603113 (2017).

[5] L. Ciorciaro, M. Kroner, K. Watanabe, T. Taniguchi, and A. Imamoglu, Observation of Magnetic Proximity Effect using Resonant Optical Spectroscopy of an Electrically Tunable $MoSe_2/CrBr_3$ Heterostructure, Phys. Rev. Lett. **124**, 197401 (2020).

[6] Y. Li, W. Zhang, V. Tyberkevych, W.-K. Kwok, A. Hoffmann, and V. Novosad, Hybrid magnonics: Physics, circuits, and applications for coherent information processing, J. Appl. Phys. **128**, 130902 (2020).

[7] E. J. Telford, A. H. Dismukes, K. Lee, M. Cheng, A. Wieteska, A. K. Bartholomew, Y.-S. Chen, X. Xu, A. N. Pasupathy, X. Zhu, C. R. Dean, and X. Roy, Layered antiferromagnetism induces large negative magnetoresistance in the van der Waals semiconductor CrSBr, Adv. Mater. **32**, 2003240 (2020).

[8] N. P. Wilson, K. Lee, J. Cenker, K. Xie, A. H. Dismukes, E. J. Telford, J. Fonseca, S. Sivakumar, C. Dean, T. Cao, X. Roy, X. Xu, and X. Zhu, Interlayer electronic coupling on demand in a 2d magnetic semiconductor, Nat. Mater. **20**, 1657 (2021).

[9] J. Klein, B. Pingault, M. Florian, M.-C. Heißenbüttel, A. Steinhoff, Z. Song, K. Torres, F. Dirnberger, J. B. Curtis, T. Deilmann, R. Dana, R. Bushati, J. Quan, J. Luxa, Z. Sofer, A. Alù, V. M. Menon, U. Wurstbauer, M. Rohlfing, P. Narang *et al.*, The bulk van der Waals layered magnet crsbr is a quasi-1d quantum material, arXiv2205.13456.

[10] F. Wu, I. Gutiérrez-Lezama, S. A. López-Paz, M. Gibertini, K. Watanabe, T. Taniguchi, F. O. von Rohr, N. Ubrig, and A. F. Morpurgo, Quasi-1d electronic transport in a 2d magnetic semiconductor, Adv. Mater. **34**, 2109759 (2022).

[11] K. Lee, A. H. Dismukes, E. J. Telford, R. A. Wiscons, J. Wang, X. Xu, C. Nuckolls, C. R. Dean, X. Roy, and X. Zhu, Magnetic order and symmetry in the 2d semiconductor CrSBr, Nano Lett. **21**, 3511 (2021).

[12] O. Göser, W. Paul, and H. Kahle, Magnetic properties of CrSBr, J. Magn. Magn. Mater. **92**, 129 (1990).

[13] W. Liu, X. Guo, J. Schwartz, H. Xie, N. U. Dhale, S. H. Sung, A. L. N. Kondusamy, X. Wang, H. Zhao, D. Berman, R. Hovden, L. Zhao, and B. Lv, A three-stage magnetic phase transition revealed in ultrahigh-quality van der Waals bulk magnet CrSBr, ACS Nano **16**, 15917 (2022).

[14] E. J. Telford, A. H. Dismukes, R. L. Dudley, R. A. Wiscons, K. Lee, J. Yu, S. Shabani, A. Scheie, K. Watanabe, T. Taniguchi, D. Xiao, A. N. Pasupathy, C. Nuckolls, X. Zhu, C. R. Dean, and X. Roy, Hidden low-temperature magnetic order revealed through magnetotransport in monolayer CrSBr, arXiv:2106.08471 (2021).

[15] S. A. López-Paz, Z. Guguchia, V. Y. Pomjakushin, C. Witteveen, A. Cervellino, H. Luetkens, N. Casati, A. F. Morpurgo, and F. O. von Rohr, Dynamic magnetic crossover at the origin of the hidden-order in van der Waals antiferromagnet CrSBr, Nat. Commun. **13**, 4745 (2022).

[16] J. Klein, Z. Song, B. Pingault, F. Dirnberger, H. Chi, J. B. Curtis, R. Dana, R. Bushati, J. Quan, L. Dekanovsky, Z. Sofer, A. Alù, V. M. Menon, J. S. Moodera, M. Lončar, P. Narang, and F. M. Ross, Sensing the local magnetic environment through optically active defects in a layered magnetic semiconductor, ACS Nano **17**, 288 (2023).

[17] S. M. Rezende, A. Azevedo, and R. L. Rodríguez-Suárez, Introduction to antiferromagnetic magnons, J. Appl. Phys. **126**, 151101 (2019).

[18] T. M. J. Cham, S. Karimeddiny, A. H. Dismukes, X. Roy, D. C. Ralph, and Y. K. Luo, Anisotropic gigahertz antiferromagnetic resonances of the easy-axis van der Waals antiferromagnet CrSBr, Nano Lett. **22**, 6716 (2022).

[19] Y. J. Bae, J. Wang, A. Scheie, J. Xu, D. G. Chica, G. M. Diederich, J. Cenker, M. E. Ziebel, Y. Bai, H. Ren, C. R. Dean, M. Delor, X. Xu, X. Roy, A. D. Kent, and X. Zhu,

Exciton-coupled coherent magnons in a 2d semiconductor, Nature (London) **609**, 282 (2022).

[20] S. Zhu and W. Zheng, Temperature-dependent phonon shifts in van der Waals crystals, J. Phys. Chem. Lett. **12**, 5261 (2021).

[21] B. Meyer, C. Elsässer, F. Lechermann, and M. Fähnle, Fortran90 program for mixed-basis pseudopotential calculations for crystals Max-Planck-Institut für Metallforschung, Stuttgart (unpublished).

[22] R. Heid and K.-P. Bohnen, Linear response in a density-functional mixed-basis approach, Phys. Rev. B **60**, R3709 (1999).

[23] D. Vanderbilt, Optimally smooth norm-conserving pseudopotentials, Phys. Rev. B **32**, 8412 (1985).

[24] J. P. Perdew, K. Burke, and M. Ernzerhof, Generalized Gradient Approximation Made Simple, Phys. Rev. Lett. **77**, 3865 (1996).

[25] H. Wang, J. Qi, and X. Qian, Electrically tunable high Curie temperature two-dimensional ferromagnetism in van der Waals layered crystals, Appl. Phys. Lett. **117**, 083102 (2020).

[26] K. Yang, G. Wang, L. Liu, D. Lu, and H. Wu, Triaxial magnetic anisotropy in the two-dimensional ferromagnetic semiconductor CrSBr, Phys. Rev. B **104**, 144416 (2021).

[27] X. Xu, X. Wang, P. Chang, X. Chen, L. Guan, and J. Tao, Strong spin-phonon coupling in two-dimensional magnetic semiconductor CrSBr, J. Phys. Chem. C **126**, 10574 (2022).

[28] I. Y. Sklyadneva, R. Heid, K.-P. Bohnen, V. Chis, V. A. Volodin, K. A. Kokh, O. E. Tereshchenko, P. M. Echenique, and E. V. Chulkov, Lattice dynamics of bismuth tellurohalides, Phys. Rev. B **86**, 094302 (2012).

[29] K. Momma and F. Izumi, Vesta 3 for three-dimensional visualization of crystal, volumetric, and morphology data, J. Appl. Crystallogr. **44**, 1272 (2011).

[30] See Supplemental Material at http://link.aps.org/supplemental/10.1103/PhysRevB.107.075421 for details on experimental setup, sample preparation, phonon modes in bulk CrSBr, and for additional Raman scattering data as a function of temperature and of an external magnetic field.

[31] M. Balkanski, R. F. Wallis, and E. Haro, Anharmonic effects in light scattering due to optical phonons in silicon, Phys. Rev. B **28**, 1928 (1983).

[32] B. A. Kolesov, How the vibrational frequency varies with temperature, J. Raman Spectrosc. **48**, 323 (2017).

[33] D. Vaclavkova, A. Delhomme, C. Faugeras, M. Potemski, A. Bogucki, J. Suffczyński, P. Kossacki, A. R. Wildes, B. Grémaud, and A. Saúl, Magnetoelastic interaction in the two-dimensional magnetic material $MnPS_3$ studied by first principles calculations and Raman experiments, 2D Mater. **7**, 035030 (2020).

[34] This behavior is also observed in a less pronounced way with phonons B^2_{2g}, A^2_{1g}, and B^3_{2g}; see Figs. S2 and S3 of Supplementary Materials [30].